Numerical Analysis of Ship Airwake on a Simplified Frigate Model

ⓘ **Tunahan Şık,** ⓘ **Uğur Oral Ünal**

Faculty of Naval Architecture and Ocean Engineering, İstanbul Technical University, İstanbul, Türkiye

Abstract

Modelling ship airwake as well as ship air resistance calculation is of great importance in ships with flight deck. Especially with a flight deck at the stern, the airwake shaped by the superstructure aerodynamics generates a complex, asymmetrical and highly turbulent form in the helicopter operation area. Within the helicopter recovery and launch operations, the turbulent area makes pilot control difficult and can even cause loss of control. It is vital to accurately evaluate the turbulence occurring in the relevant region in order to increase operational efficiency, prevent possible accidents and reduce pilot workload. In this study, the effect of the flow regime in the flight deck airborne on a simple frigate shape has been examined with computational fluid dynamics using scale-resolving simulations. The results have been exhibited a remarkable agreement with the experimental data, and it has been agreed that the solution method could be a priority in ship airwake calculations.

Keywords: Ship aerodynamics, ship airwake, turbulence, computational fluid dynamics (CFD), scale-resolving simulations (SRS), simple frigate shape 2 (SFS2)

1. Introduction

In ship construction, aerodynamic design is often overlooked due to the relatively lower contribution of air resistance to the overall resistance of the vessel. While aerodynamic considerations are more critical for yachts, they are not typically prioritized for commercial and military ships. In modern military ship design, the superstructures are primarily shaped to minimize radar visibility, with less emphasis on aerodynamic efficiency. These enclosed, bluff-body designs significantly impact the ship's air resistance and have a considerable influence on the flow characteristics over the vessel.

In ships with helicopter decks, such as large naval ships, mega yachts, research ships, and drilling platforms; besides considering the air resistance, calculation of the airwake over the flight deck are of great importance. Particularly in ships with stern flight decks, the airflow, shaped by the superstructure, directly influences the flight operations by forming a complex turbulent wake over the deck.

The relative airflow over the flight deck created by the ship's own motion and the external wind flow, is the main factor driving the airwake formation. Additional elements, such as the thermodynamic effects of air temperature and exhaust gases, contribute to the complexity of the airwake. These bluff superstructures, along with various systems and equipment mounted on them (such as antennas, radars, funnels, and weapon systems), further complicate the already asymmetric flow regime. This turbulent environment, characterized by various multi-directional vortices, causes sudden pressure differences at both low and high frequencies, which result in a significant increase in the pilot's workload. Especially within the ratchet frequency range of 2-3 Hz, helicopter control

Address for Correspondence: Tunahan Şık, Faculty of Naval Architecture and Ocean Engineering, İstanbul Technical University, İstanbul, Türkiye
E-mail: sikt21@itu.edu.tr
ORCID ID: orcid.org/0009-0008-7752-2583

becomes difficult [1]. In bad weather and sea conditions, these situations can even lead to crashes. Given the high intensity of flight operations on naval ships and the importance of manoeuvre efficiency and time, it is extremely important to include airwake calculations during the design phase and implement related aerodynamic structural improvements.

Given the presence of high vortices and turbulence over a simple ship form, the resulting airwake becomes complex, and each ship exhibits distinct flow characteristics, making airwake interpretation a challenging task. To date, the interpretation of airwake has been conducted using in situ measurements taken on ships, low-speed wind tunnel experiments, and flow-resolving simulations.

In-situ tests, also known as sea trials, began in the mid-1950s, but due to operational costs, time-consuming processes, and military secrecy, they are rarely mentioned in the literature. Instead, tests verified by wind tunnel experiments have been more common.

In the early 1960s, wind tunnels started to be used alongside the first computational fluid dynamics (CFD) simulations introduced by Mahaffey et al. [2]. It is known that CFD studies verified with experimental data are more practical during the early design stages of a ship. As computational capacity and code capabilities have improved, CFD has become a crucial component for ship-helicopter dynamic interface (SHDI) calculations.

Notable ship forms frequently used in the literature include the Canadian Patrol Frigate (CPF), the UK's Duke-class Type 23 frigate (T23), the simple frigate shape (SFS1) and revised SFS1 (SFS2).

Zan et al. [3], and Zan [4,5] worked on airwake analysis for CPF using both low-speed wind tunnel experiments and CFD at the National Research Council of Canada (NRC) Aerodynamics Laboratory. The numerical results were consistent with the experimental results from the simplified CPF model, providing valuable insights into airwake calculations. Later, Syms [6] conducted time-independent CFD simulations (Reynolds-Averaged Navier-Stokes, RANS) for various wind angles. When compared with experimental results, RANS successfully captured the main flow characteristics but exhibited higher gradients. Similarly, Yuan et al. [7,8] compared their CFD studies using delayed detached-eddy simulation (DDES) models in OpenFOAM with experimental data from CPF, demonstrating the effectiveness of the code in simulating unsteady airflows over ships. Furthermore, to include ship motion, Yuan et al. [9] placed the CPF model on a multi-degree of freedom system in a wind tunnel. They found that OpenFOAM was able to solve the airflows, which became more unstable with ship movements.

In NATO workshops, as part of The Technical Cooperation Program, Cheney and Zan [10] introduced the SFS1 geometry and carried out CFD studies alongside wind tunnel experiments at the NRC. Subsequently, Reddy et al. [11] shared their RANS simulations on SFS1, demonstrating the consistency of the results with experimental data. They observed that vortices dominated the flow field in the region of interest and noted differences in the position of the reattachment point. Similarly, Wakefield et al. [12] developed a CFD model for the combination of a helicopter rotor and SFS1, commenting that the induced velocity gradients around the rotor increased the force required to keep the helicopter in a specific position. Experimentally, Bardera-Mora [13] conducted tests on SFS1 using laser Doppler anemometry (LDA) and particle image velocimetry (PIV) at the National Institute of Aerospace Technology in Spain. They observed a horseshoe-shaped vortex structure forming in front of the hangar. Lindon and Thornber [14] used SFS1 to propose a method for quantifying uncertainties due to rounding and truncation errors caused by the finite-difference approach in CFD. To ensure statistical accuracy in simulation time, they developed a formula for a stopping criterion based on pre-defined requirements. Additionally, Zamiri and Chung [15] conducted a DDES-based study on SFS1, applying flow from seven different wind angles. They reported that as the wind angle increased, the turbulence kinetic energy over the ship increased, and the flow field became more asymmetric.

The first study to compare SFS1 and SFS2 was conducted by Syms [16]. He used the experimental results provided by NRC to validate his study and compared the bodies using the Lattice-Boltzmann flow solver in the PowerFLOW code. The results demonstrated that the Lattice-Boltzmann method could accurately capture the flow topology. He pointed out that SFS2 has more realistic results with its bow shape than SFS1 because it represents a closer geometry to a frigate. There after many studies have focused on the SFS2 body instead of SFS1.

Zhang et al. [17] performed time-dependent simulations on SFS2 using the Cobalt solver with Euler formulation. They also used the NRC data for CFD validation. The computed data showed acceptable agreement with experimental data. Again based on the NRC data, Forrest and Owen [18] conducted a comprehensive study on SFS2 using DDES, examining a simplified T23 frigate model under various wind angles. They observed that DDES could model large-scale turbulent structures in a remarkable manner. Forrest et al. [19,20] further explored the effects of modifications to the vertical hangar edge on airwake characteristics using DDES with ANSYS-Fluent, noting that two out of five modifications provided beneficial effects while the other

three increased the pilot workload. Similarly, Kääriä et al. [21] applied six different modifications to the superstructure corner of a Simple Research Frigate model and tested them in a wind tunnel. Their study showed that the modifications directly impacted the airwake region and that certain modifications reduced turbulence intensity in the helicopter manoeuvring area. For further detailed information on the history of airwake calculations and their analysis, it is worth reviewing the study of Shukla et al. [22]. Turbulence models and simulations commonly used in airwake studies include RANS, unsteady RANS (URANS), scale-adaptive simulation (SAS), detached-eddy simulation (DES), and delayed DDES. Shukla et al. [23] performed CFD analysis using the scale-adaptive simulation (SAS) turbulence model on SFS2, comparing the results with NRC data. Subsequently, they conducted a wind tunnel test, comparing URANS, SAS, and DES models [24,25]. They concluded that DES and SAS closely matched experimental data, with SAS offering solutions for large-scale turbulent structures at lower computational costs.

In consideration of this information, accurately assessing turbulence in the region of interest is essential for improving operational efficiency, reducing pilot workload, and preventing potential accidents and damage. Accordingly, this study focuses on calculating the ship airwake, which represents the initial step in ship-helicopter interaction studies, and aims to establish a foundation for airwake calculations using CFD.

Based on previous research, it has been concluded that scale-resolving simulations (SRS) offer an effective approach to resolving the turbulent structures generated by bluff bodies, such as ship superstructures, which induce significant flow separations. Though, a review of the literature reveals that the critical computational steps necessary for accurately capturing flow structures, particularly turbulence intensity, using different SRS techniques have not been clearly defined. Thus, this study aims to present a comprehensive computational strategy for effectively and reliably conducting ship airwake simulations using advanced SRS methods.

In addition to the commonly employed SRS models, this study incorporates the stress-blended eddy simulation (SBES) model, which has been introduced in recent studies but has not yet been applied to ship airwake calculations. By comparing the computational results with experimental data available in the literature, this study demonstrates the predictive capabilities of these methods for complex separated flows characterized by high levels of vorticity and turbulence. It serves as a roadmap for researchers interested in advancing this field.

2. Scale-Resolving Simulations

Principally, RANS equations can undoubtedly be solved in a time-dependent manner (URANS). However, classic turbulence models, while sufficient for time-step resolution, are insufficient to accurately predict high-vorticity and turbulence levels in complex flows where significant flow separation occurs. SRS, which have been developed to address this deficiency, offer results closer to experimental data.

Commonly used SRS techniques such as large eddy simulation (LES), DES, DDES, and SAS have been further developed over time. These have been followed by improved DDES (IDDES), shielded DES (SDES), and more recently, SBES.

Among these, LES is considered the most effective alternative to direct numerical simulation (DNS) for solving vortex dynamics. Due to its wide applicability and high accuracy, LES is often preferred for industrial applications. However, LES solutions require very small time steps and highly refined mesh grids, significantly increasing computational time and cost. Recent studies have focused on finding more practical and efficient solutions to this phenomenon.

Menter and Egorov [26], Egorov et al. [27] introduced the SAS concept by including the von Kármán length scale in the RANS turbulence equations. The von Kármán length scale enables SAS to dynamically adjust to the unsteady regions of the flow, behaving like LES in regions of high instability. In stable regions, it behaves like standard RANS models, providing a broad range of turbulence solutions for certain types of unsteady flows. The two-equation formulation for SAS, where "L_{vK}" represents the von Kármán length scale, is shown below:

$$\frac{\partial(\rho k)}{\partial t} + \frac{\partial(\rho \bar{U}_j k)}{\partial x_j} = P_k - c_\mu^{3/4} \rho \frac{k}{\Phi^2} + \frac{\partial}{\partial x_j}\left(\frac{\mu_t}{\sigma_k}\frac{\partial k}{\partial x_j}\right) \qquad (1)$$

$$\frac{\partial(\rho \Phi)}{\partial t} + \frac{\partial(\rho \bar{U}_j \Phi)}{\partial x_j} = \frac{\Phi}{k} P_k \left(\zeta_1 - \zeta_2 \left(\frac{L_t}{L_{vK}}\right)^2\right)$$
$$- \zeta_3 \rho k + \frac{\partial}{\partial x_j}\left(\frac{\mu_t}{\sigma_\Phi}\frac{\partial \Phi}{\partial x_j}\right) \qquad (2)$$

In contrast to SAS, a family of hybrid simulation models has been developed, directly benefiting from LES while maintaining RANS efficiency. These simulations, which transition between RANS and LES, include models like DES, DDES, IDDES, SDES, and SBES. Hybrid models are powerful formulations for resolving turbulence in unstable regions, such as those found in flight envelopes. While

applying a standard RANS model in these regions can result in single-frequency vortex formation, hybrid models allow large structures to be broken down into smaller scales. Additionally, they can model smaller vortices near the boundary layers while preventing excessive resolution requirements, allowing RANS solutions in boundary layers.

The first hybrid simulation, DES, developed by Spalart et al. [28], and Spalart [29], enabled a transition between RANS and LES. In this formulation, boundary layers near walls are fully modelled by RANS, while free flows away from the walls are modelled by LES. This relatively simple mathematical formulation can be built on top of any existing RANS turbulence model. DES has garnered significant interest by turbulence communities as the first and highly effective SRS method.

Following the proposal by Menter and Kuntz [30] to protect boundary layer separation near walls, Spalart et al. [31] further developed DES into the DDES. The formulation for DDES includes a protection function that equals "1" inside the boundary layer and "0" outside of it:

$$E_{DES} = \rho \frac{k^{3/2}}{L_t} \max\left(1; \frac{L_t}{C_{DES}\Delta}\right) \longrightarrow$$

$$E_{DDES} = \rho \frac{k^{3/2}}{L_t} \max\left(1; \frac{L_t}{C_{DES}\Delta}(1 - F_{DDES})\right) \qquad (3)$$

As it became clear that preserving boundary layer solutions near walls led to more effective results in CFD applications, DDES evolved further into the SDES and eventually into SBES, developed by Menter [32]. In SBES, unlike previous models, the protection function is adjusted based on the stress level:

$$\tau_{ij} = \tau_{ij}^{RANS} f_s + \tau_{ij}^{LES}(1 - f_s) \qquad (4)$$

$$\mu_t = \mu_t^{RANS} f_s + \mu_t^{LES}(1 - f_s) \qquad (5)$$

SBES is believed to provide stronger protection of the boundary layer compared to DES/DDES, allowing for a faster transition between RANS and LES models.

The following points stand out regarding the use of SRS models in [32,33]:

1. SAS is considered the most reliable SRS method when dealing with coarse grids where the mesh resolution required for LES cannot be achieved.

2. In cases where SAS is insufficient, increasing the grid resolution and applying DDES provides better results.

3. SBES can be used more broadly for a variety of complex problems.

4. The Courant-Friedrichs-Lewy (CFL) number should be kept around "1" or below for all SRS methods.

3. Computational Study

The validation of the computational analyses was based on the low-speed wind tunnel experimental data of the NRC by Lee [34] in 2007. The experiments examined the effect of the flow regime on the helicopter deck of the commonly used ship geometry, the SFS2 (Figure 1).

The test section of the tunnel has dimensions of 1.9 m × 2.7 m × 5.2 m, with a turbulence intensity of 0.14%. To ensure accuracy in the computational solution, the SFS2 geometry and the flow field were modelled at a 1:100 scale, identical to the experimental setup, and matched to the dimensions of the wind tunnel as seen in Figure 2. Two different wind angles were analysed, one from the bow (0°) and one at 45° from the starboard side, as in the experiment.

The DDES model, commonly used in airwake studies, has shown close agreement with experimental data in prior researches. While there have been limited applications of
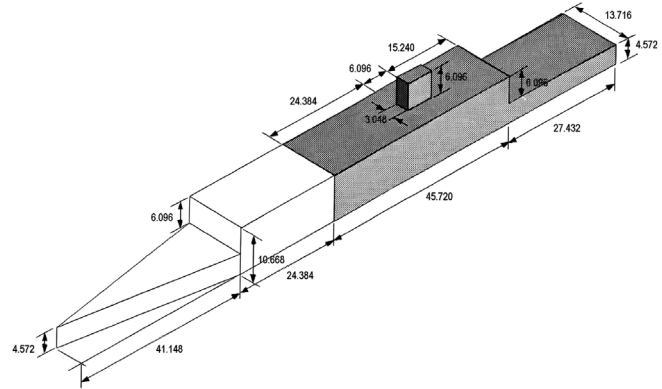

Figure 1. SFS2 Model (Dimensions are in meters; the shaded section represents SFS1) [5].
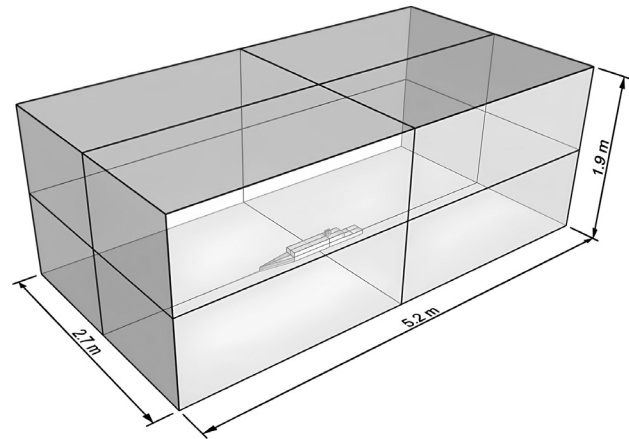

Figure 2. 1:100 scale SFS2 model geometry located in the middle bottom of the flow field.

URANS and SAS, SBES has not yet been used in any ship airwake study. It is known that geometries causing high levels of flow separation, such as the transition between the hangar and helicopter deck, lead to rapid transitions to turbulence from the boundary layer. Therefore, considering the previously mentioned SRS models, it was determined that using SBES, which transitions rapidly between RANS and LES, would be meaningful.

In this survey, a comparison of the URANS, SAS, DDES, and SBES simulation techniques was conducted to establish a baseline for airwake calculations using CFD.

3.1. Mesh and Boundary Layer Approach

A method based on "cutcell", which reduces the cells in size by powers of two, was used for the mesh generation. The mesh structure was refined around the region of interest (the helicopter operation area) where the airwake was examined, as seen in Figure 3, as well as around the funnel where turbulence was expected to increase. A smooth transition was ensured between the hexagonal cells used on the surfaces and the cubic cells used in the flow field. Since cubic and hexagonal cells were used, the aspect ratio was approximately 1:1 in 90% of the total mesh, and below 20 for the rest.

The number of cells required in the boundary layer depends on the type of flow and the accuracy required. In high-Reynolds-number flows, such as in aerospace studies, where high accuracy is needed, the number of cells in the boundary layer perpendicular to the wall is typically around 40-50. However, in many industrial applications, 10 cells are considered sufficient.

Additionally, there are many flow problems where reasonable solutions can be achieved with fewer cells, often only 3-5 layers. The common feature of these problems is that the main flow phenomenon occurs outside the boundary layer due to flow separation. Yuan et al. [8] highlighted that, in airwake studies, the flow is primarily driven by inertial forces, and separation points are more influenced by sharp edges and corners than by boundary layer separation. Accordingly, it was determined that it was not necessary to fully resolve the boundary layer with RANS calculations in this study.
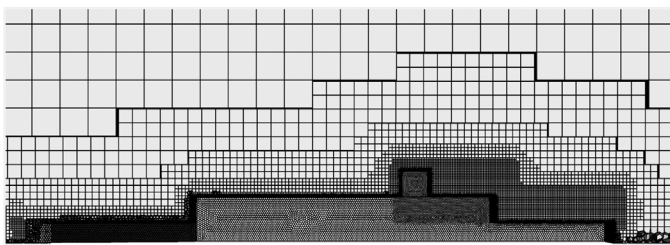

Figure 3. 1:100 scale SFS2 model geometry located in the middle bottom of the flow field.

Therefore, it was concluded that a detailed boundary layer solution over the ship's geometry with discontinuities was unnecessary. However, the CFL number needed to be kept close to 1, especially in target regions. Spectral analysis and detailed problem resolution require both small time steps and high mesh resolution in regions where LES is applied. Thus, the cell aspect ratio was kept close to 1 both inside and outside the boundary layer, and 3 boundary sublayers were used in the direction normal to the wall. For each solution, the y^+ value was kept around 50. Additional studies confirmed that maintaining a y^+ value of 1 did not significantly alter the results for this problem.

3.2. Initial, Boundary Conditions and Timing

At the inlet boundary, a flow speed of 60 m/s was specified for the 0° wind angle and 50 m/s for the 45° wind angle. The turbulence intensity was set to 0.14%, and the turbulence length scale was defined as 4.3b (b, ship's width) according to the reference experimental study. No-slip wall condition was applied for the lateral boundaries, and atmospheric pressure was specified at the outlet boundary.

In the experimental study [34], data were collected at a frequency of 2 kHz. Not to exceed the equivalent time step size (5×10^{-4}) and to keep the CFL number below 1 in the region of interest, the time step sizes for the study used are 1.3×10^{-4}, 1×10^{-4}, 7×10^{-5} s respectively for the meshes A, B and C.

Before the time-dependent solution was initiated, a steady-state solution was performed to achieve early convergence. The results of the steady-state simulation were used as initial conditions for the time-dependent simulation. In terms of pressure-velocity coupling, the equations were solved in the "Coupled" method for the first ~10 time steps, then the "SIMPLE" method was applied in continuation. It was observed that 10 iterations per time step were sufficient. The data acquisition was started after the solutions reached iterative stability at about 5×10^{-2} s, therefore the earlier data was disregarded.

3.3. Data Acquisition

In the experimental wind tunnel test, each measurement lasted for 16.4 s. In this study, the simulation time was extended beyond this duration, with at least 20 s of measurement for each solution. The acquired data were used for the power spectral density (PSD) calculations through Fourier transformation.

Measurements were taken over the flight deck, with data points placed at the "hover" position above the hangar edge, where a helicopter would be during launch or recovery operations. To observe the pressure and velocity distributions, four planes were positioned starting from the ship's stern and extending toward the bow at intervals of one-quarter of

the platform length (L_p) and having a width of 2 times ship beam. These planes were aligned along the ship's centreline from their mid-section and were positioned at a height along the hangar halfway, with a total height equal to 75% of the hangar height (h). The planes were named "0% L_p, 25% L_p, 50% L_p and 75% L_p" respectively towards the bow. Linear data measurements made at the level of the hangar upper edge line on the planes are expressed such as "25% L_p line".

Spectral velocity measurements were acquired from two locations: for the 0° wind angle, from the point which is located at h/4 height from the bottom line of 50% L_p plane, 2b/5 to the starboard side from the centreline and for the 45° wind angle from the point on 25% L_p. Those were named "50% L_p spectrum point" and "25% L_p spectrum point," respectively.

The formula used to calculate turbulence intensity is shown below, where "k" represents turbulence kinetic energy, "U_∞" is the free-stream velocity, and "u', v', w'" represent the Reynolds decomposition components:

$$I(\%) = \frac{100}{U_\infty} \sqrt{\frac{2}{3}k} \qquad (6)$$

$$k = \frac{1}{2}((\overline{u'})^2 + (\overline{v'})^2 + (\overline{w'})^2) \qquad (7)$$

3.4. Mesh Independence Analysis

The mesh independence study was conducted using the SBES method. Three different mesh densities were used:
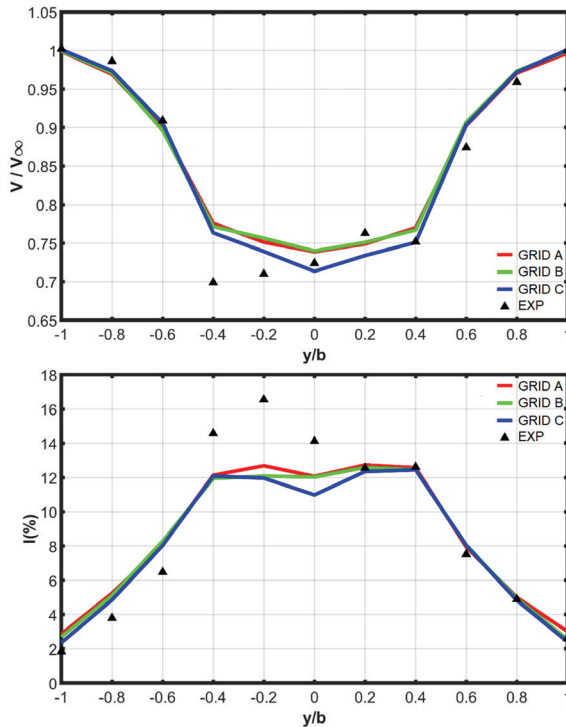

Figure 4. Comparison of mean velocity magnitude (up) and turbulence intensity distribution along the 50% L_p line for the grids.

coarse, medium, and fine, named Grid A, Grid B, and Grid C, respectively. The cell sizes in the region of interest were refined in this order for LES computations, while they were kept constant for outer cells. The smallest cube-shaped cell edge dimensions (Δ_0), which are normalized by the hangar height (h) and reduced in multiples of $\sqrt[3]{2}$, and the total number of cells are presented in Table 1.

The results of the simulations in 1 s of duration were considered sufficient for the mesh independence analysis since the solutions had been observed to stabilize after 50 ms. Figure 4 shows the mean velocity magnitude and mean turbulence intensity distributions. The experimental results [34] are labelled as "EXP" in the figure and the comparisons are also presented in Table 1. The relative error values in the table were calculated individually for each point by comparing the computed results with the corresponding experimental data, then the mean error values were taken.

Although both Grid A and Grid B produced nearly identical results for velocity magnitude, Grid C yielded slightly more accurate results. As expected, finer grids provided better results for turbulence intensity. However, given that the total number of cells in Grid C was four times that of Grid B, the ~1% difference in relative error was considered negligible in terms of time and computational efficiency. Therefore, the simulations were continued using Grid B.

4. Results and Discussion

The comparison for the 0° case also included a study conducted by Forrest and Owen [18] at the University of Liverpool using the DDES method, labelled as "LIV". The experimental results [34] are labelled as "EXP". The x-axis denoteas the non-dimensionalized lateral position normalized by the ship's beam in the graphs representing the mean velocity magnitude and turbulence intensity across the section. Both the velocity and turbulence intensity values were non-dimensionalized by the free-stream velocity.

Table 1. Comparison of the grid characteristics and relative error for velocity magnitude and turbulence intensity.

	Grid A	Grid B	Grid C
Δ_0/h (x 10^{-2})	7.2	5.7	4.6
Total cell count (x 10^6)	0.36	0.40	1.3
Relative error in velocity magnitude (%)	2.8	2.8	2.3
Relative error in turbulence intensity (%)	18.0	16.4	15.0

4.1. Comparative Performance Assessments of the Simulations

Table 2 presents the relative error values for velocity magnitude and turbulence intensity distributions seen in Figure 5. These errors were calculated individually for each point by comparing the simulation results with the corresponding experimental data, and the average error for each method was reported.

As shown in Table 2, the URANS method produced the poorest results, particularly for turbulence intensity. While SAS performed relatively better in predicting velocity magnitude, its performance in predicting turbulence intensity was inferior to that of DDES and SBES. Although the results from SAS, DDES, and SBES were relatively close to each other, they significantly outperformed the LIV results in terms of turbulence intensity. Considering the turbulence intensity that forms the basis of ship airwake studies, DDES and SBES have produced results that are closer to experimental data compared to SAS. For velocity magnitude, DDES and SBES yielded nearly identical results. Only minor

differences were observed in turbulence intensity predictions of these simulations.

Given the importance of PSD distribution in flight envelope calculations, it is essential to compare the performance of DDES and SBES in spectral analyses. Figure 6 shows the spectral density distributions obtained using Fourier transformation, where the frequency and amplitude are presented on a logarithmic scale. In the spectral analysis, the longitudinal PSD values were closer to the experimental results compared to the lateral PSD values. At low frequencies, the differences between the simulation methods were negligible. However, at higher frequencies, SBES produced results closer to the experimental data. In the longitudinal spectrum, SBES showed a closer match to the experimental data at low frequencies, while following similar pattern at high frequencies, consistent with the lateral spectrum. Although DDES and SBES produced similar results for velocity magnitude and turbulence intensity, their differences become more pronounced in the spectral
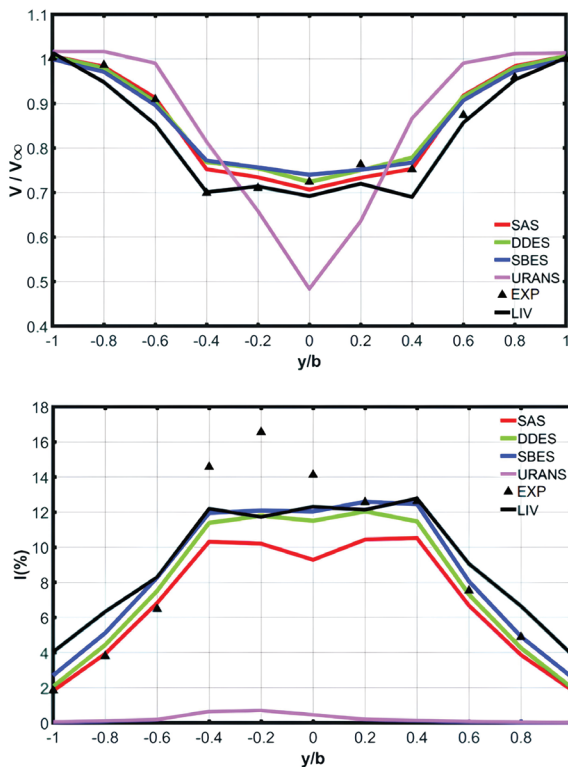

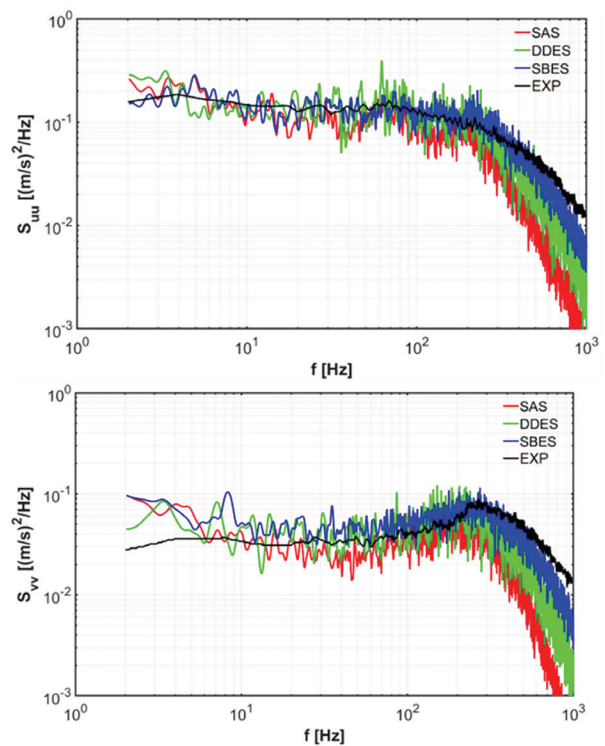**Figure 5.** Comparison of mean velocity magnitude (up) and turbulence intensity distribution across the 50% L_p line.

Figure 6. Comparison of longitudinal (up) and lateral PSD on the 50% L_p spectrum point for 0°.

Table 2. Comparison of relative errors in velocity and turbulence intensity.					
Relative error (%)	**LIV**	**URANS**	**SAS**	**DDES**	**SBES**
Velocity Magnitude	3.0	11.1	2.4	2.8	2.8
Turbulence Intensity	34.7	97.6	18.8	15.1	16.4

analysis. As expected, SBES provided the most accurate results; therefore, the simulations were continued using this method.

Figure 7 illustrates the vortex structures using the Q-criterion [35] at the end of the first second of the solution. The SBES method provided a more detailed and comprehensive solution in the region of interest compared to the other methods.
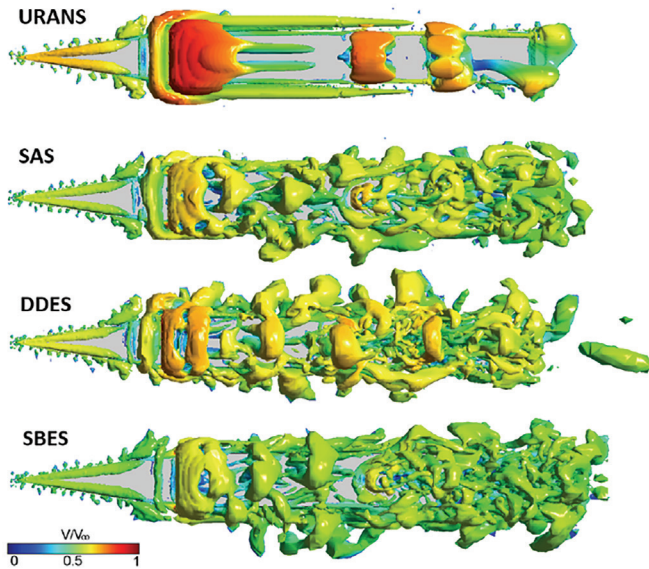

Figure 7. Comparison based on Q criterion (Q=0.1; vortex colorization is based on velocity magnitude).

4.2. SBES Methodology and Comparative Flow Direction Evaluations

4.2.1. 0° flow direction

For all results, experimental data [34] is labelled as "EXP", and the SBES simulation results as "CFD". The colours represent the velocity values non-dimensionalized by the free-stream velocity. The flow field resulting from the head direction flow was compared with the experimental data on the data planes. The longitudinal and lateral velocity distributions are shown in Figure 8. As seen in the comparison of the calculated data along the 50% L_p line in terms of velocity and turbulence intensity above, a similar relative error (15-20%) can also be observed here when looking at the planes they are located on.

The primary factors causing the discrepancies between the experimental and computational results were considered to be experimental measurement errors, computational method limitations, and mesh resolution. As noted in the mesh independence section, the resolution of the mesh impacted the accuracy of the results, with finer meshes providing closer agreement with experimental data.

4.2.2. S45° flow direction

For the 45° flow angle from the starboard side (S45°), the velocity distributions across the data planes were compared with the experimental data [34]. The longitudinal and lateral velocity distributions are presented in Figure 9. The velocity values are non-dimensionalized by the free-stream velocity.
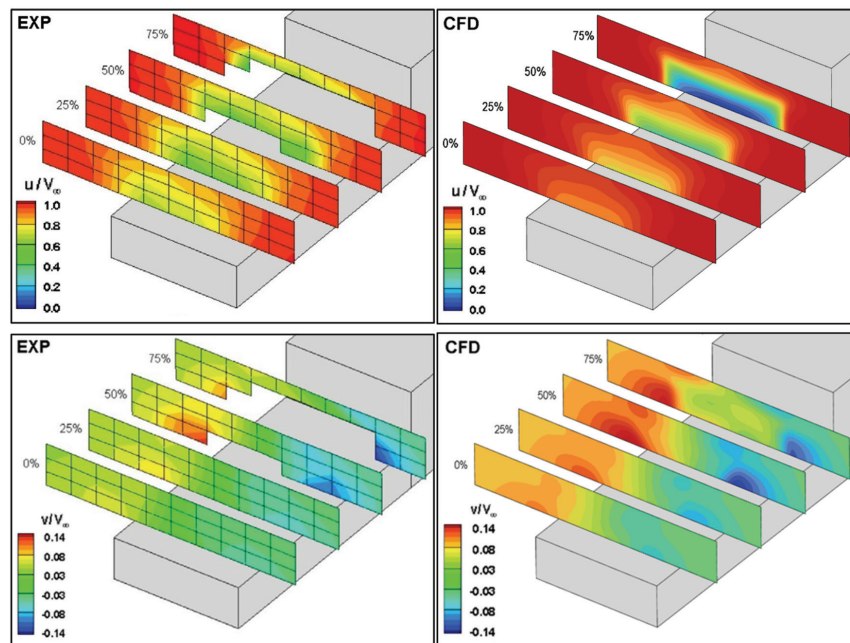

Figure 8. Comparison of longitudinal (up) and lateral velocity distributions on the data planes for 0°.
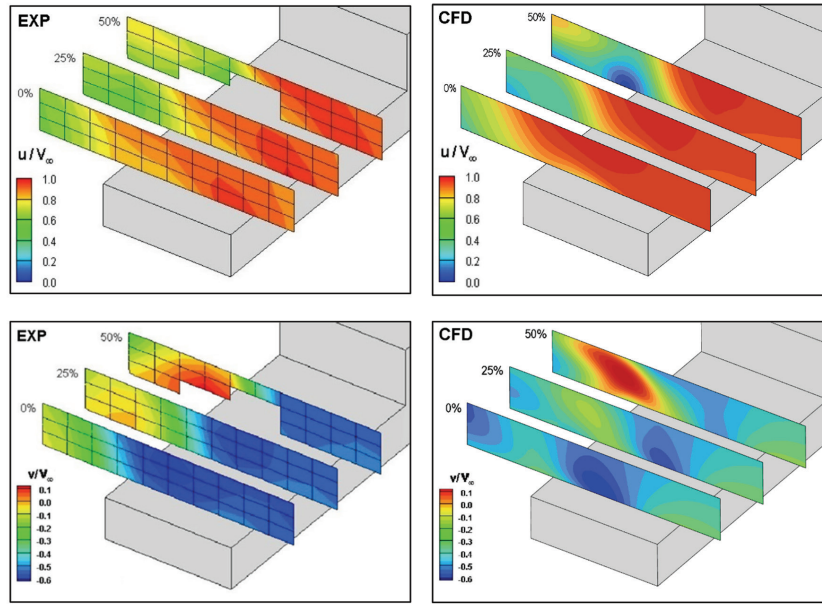
Figure 9. Comparison of longitudinal (up) and lateral velocity distributions on the data planes for S45°.

While the superstructure of the ship interacts with the flow primarily from the bow with the bridge and funnel in the 0° case, the S45° case additionally includes the structure from the starboard side, increasing the cross-sectional area exposed to the flow. As a result, the turbulence kinetic energy over the ship increases, and the flow field becomes much more asymmetric. This makes it more challenging to predict the wake region accurately with computational methods. As seen in the comparison of the calculated data along the 50% L_p line for the S45° case in terms of velocity and turbulence intensity above, a similar relative error (30%) can also be observed here in Figure 9 when looking at the planes they are located on.

4.2.3. 0° and S45° flow directions comparison

A comparison of the average velocity magnitude contours and streamlines for the 0° and S45° cases on a plane located
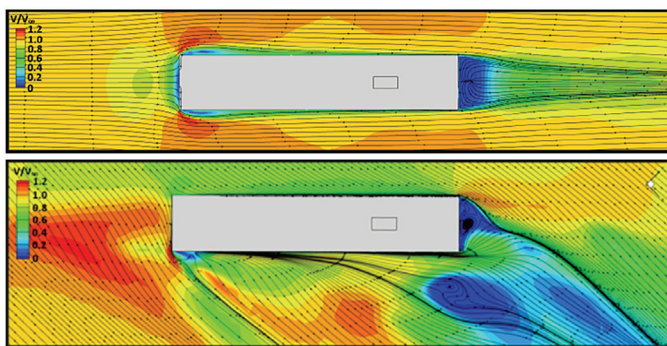
75% of the hangar height is shown in Figure 10. In the 0° case, the flow decelerates to nearly a complete stop around the bridge region. As the flow accelerates again towards the flight deck, it experiences a reduction in velocity due to the discontinuity in the superstructure. The S45° case presents a more pronounced reduction in velocity on the leeward side of the superstructure. Additionally, the increased complexity of the flow in the wake region of the S45° case is characterized by the presence of multiple independent vortices, which are not observed in the 0° case.

Figure 11 shows the distribution of vortices over the ship for the both cases, visualized using the Q-criterion [35]. The vortex structures formed at the bow and bridge are more pronounced in the S45° case, where the starboard side of the
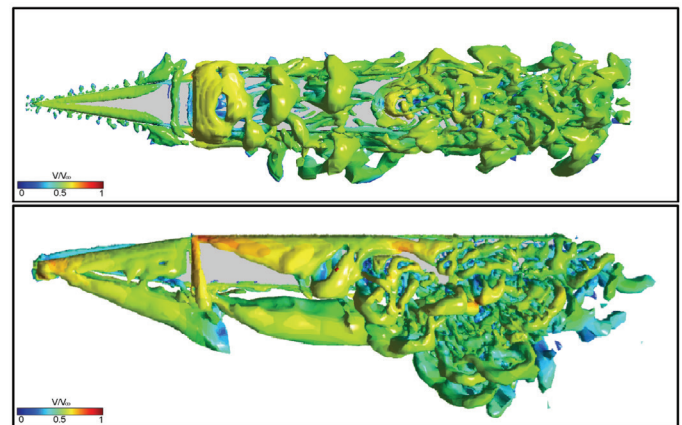

Figure 10. Mean velocity magnitude contours and streamlines for 0° (up) and S45° occurred at 75% of hangar height line (results based on the SBES method).

Figure 11. Comparison of the Q-criterion vortex distribution for 0° (up) and 45° flows (Q=0.1, vortex colorization is based on velocity magnitude; results based on the SBES method).
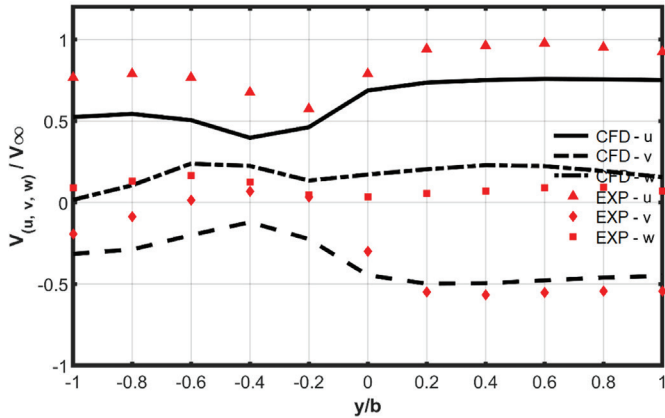
Figure 12. Distribution of velocity components on the 50% L_p line for 0° (up) and S45°
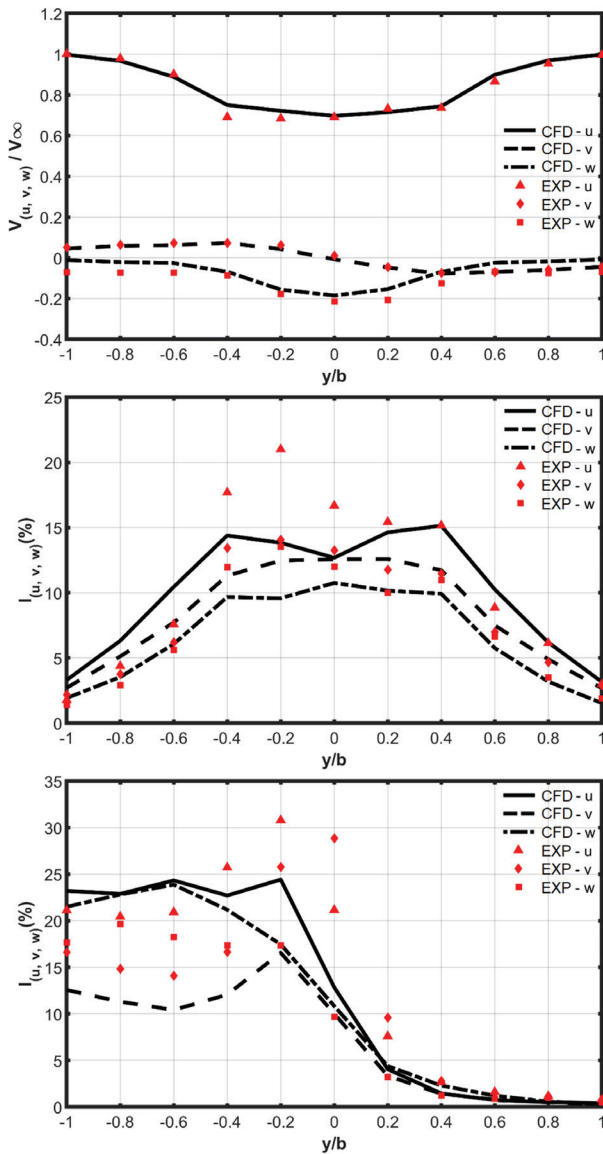

Figure 13. Distribution of turbulence intensity on the 50% L_p line for 0° (up) and S45° flow directions.

superstructure also contributes to the formation of additional vortices. A 30% increase in vorticity is observed in the S45° case compared to the 0° case.

Non-dimensional distributions of mean velocity magnitude and turbulence intensity for the 0° and S45° flow directions are presented in Figures 12 and 13 respectively. As mentioned previously, the results show that while the superstructure interacts with the flow primarily at the bow in the 0° case, the S45° case introduces the starboard side of the superstructure into the flow, making the wake region more complex and difficult to interpret computationally. Consequently, while the simulated results show good agreement with the experimental data in the 0° case, the complexity of the wake region results in a less precise correlation between the simulation and the experimental data in the S45° case. Nevertheless, it can be said that the results follow a similar trend.

Figures 14 and 15 show the longitudinal and lateral PSD distributions for the 0° and S45° flow directions, respectively. The PSD values for the head flow case are in close agreement with the experimental results, while the results for the S45° case exhibit larger discrepancies, particularly at frequencies above approximately 100 Hz for both longitudinal and lateral components.
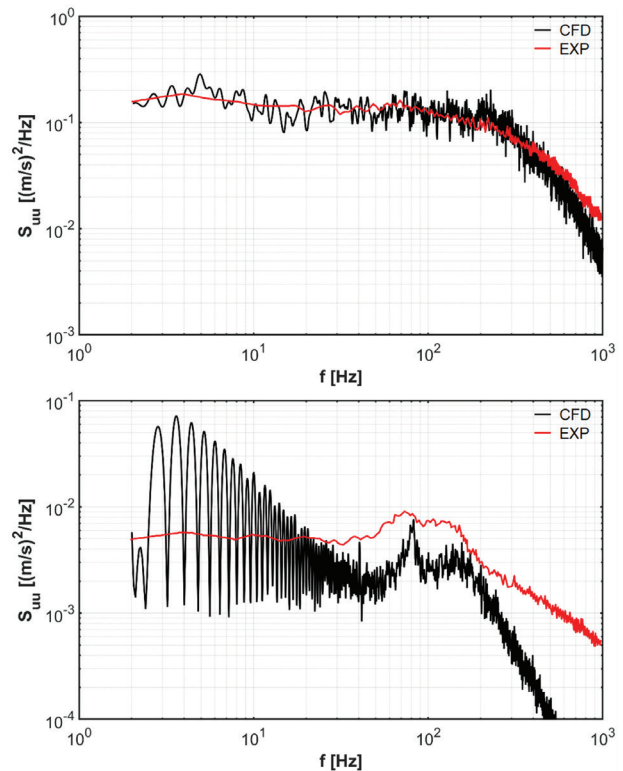

Figure 14. Longitudinal PSD comparison at the 50% L_p spectrum point for 0° (up) and at the 25% L_p for S45°.

5. Conclusions and Future Work

This study presents a comprehensive computational strategy for the effective and accurate calculation of ship airwake. SRS techniques, which have gained popularity in recent years, were applied and compared against experimental data from the literature. The predictive capabilities of these methods were evaluated in detail.

Primarily, all SRS methods demonstrated significantly superior results in terms of velocity magnitudes and turbulence intensity levels compared to URANS. For velocity magnitude, SRS methods yielded results within a ~1% difference from each other. However, predictions of turbulence intensity varied by ~1-4%, depending on the simulation technique employed. Notably, the DDES and SBES models predicted turbulence intensity within ~15% and ~16% of the experimental values, respectively. In spectral analyses, which are crucial for assessing flight envelope characteristics, SBES exhibited greater alignment with experimental results, particularly in the high-frequency ranges, where it demonstrated approximately 50% greater accuracy compared to DDES. This improvement is attributed to SBES' faster transition to LES resolution, leading to better performance in turbulent flow regions.

Key findings from this study are as follows:

Figure 15. Lateral PSD comparison at the 50% L_p spectrum point for 0° (up) and at the 25% L_p for S45°.

- The detailed comparisons showed that SRS methods are highly effective in modelling turbulence, especially in the regions with high levels of flow separation occurring on discontinuous ship superstructure.

- Increasing the mesh resolution in the helicopter flight zone improved the accuracy of the results. This confirms that grid refinement, particularly in critical flow regions, plays an important role in capturing turbulence structures.

- The computational load was reduced by adopting a simplified boundary layer modelling approach, while conserving the accuracy of the airwake simulations. However, it was seen that ~1% refinement of the solution accuracy in terms of turbulence intensity costed 4 times higher cell count. Thus, there should be a balanced approach while determining the grid for entire solutions as it is a trade-off between solution accuracy and time efficiency.

- Using optimal time step values ensured that there is no need to perform additional time dependence studies.

- The computational strategy resulted in effective and reliable outcomes with relatively less resource usage, making the methods suitable for ship airwake simulations critical to SHDI studies.

- It is concluded that SBES, which has been used in recent studies for different types of analyses, can also be used as a primary method for ship airwake calculations.

For future studies, the focus will be on achieving aerodynamic improvements in the ship's airwake through various design applications, examining the effects of the atmospheric boundary layer, incorporating six degrees of freedom for ship motion, and conducting both numerical and experimental airwake analyses on more detailed ship geometries. By continuing this line of research, it will be possible to further enhance the accuracy of airwake predictions, ultimately contributing to the design of safer and more efficient ship-aircraft interaction systems for future naval and commercial platforms.

Footnotes

Authorship Contributions

Concept/Design: T. Şık, Data Collection or Processing: T. Şık, Analysis or Interpretation: T. Şık, and U. O. Ünal., Literature Review: T. Şık, Writing, Reviewing and Editing: T. Şık, and U. O. Ünal.

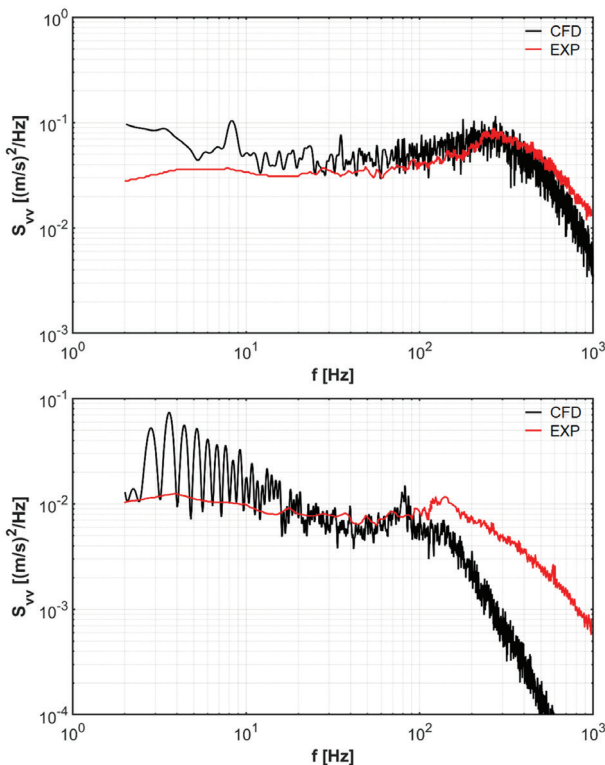**Conflict of Interest:** No conflict of interest was declared by the authors.

6. References

[1] D. E. Johnston and D. T. McRuer, "Investigation of interactions between limb-manipulator dynamics and effective vehicle roll control characteristics", *NASA CR-3983*, 1986.

[2] W. Mahaffey, T. Mukerjee and A. Singhal, "Prediction of turbulent ship air-wake characteristics", *Numerical Simulation of Fluid Flow and Heat/Mass Transfer Processes*. Lecture Notes in Engineering, Springer, Berlin, Heidelberg. vol. 18, 1986.

[3] S. J. Zan, J. F. Syms and B. T., Cheney, "Analysis of patrol frigate air wakes", *Fluid Dynamics Problems of Vehicles Operating Near or in the Air-Sea Interface*, RTO-MP-15, Paper 7, RTO/NATO, Amsterdam, 1998.

[4] S. J. Zan, "Experimental determination of rotor thrust in a ship airwake", *American Helicopter Society*, vol. 47, no. 2, pp. 100-108, 2002.

[5] S. J. Zan, "On aerodynamic modelling and simulation of the dynamic interface", *Journal of Aerospace Engineering*, Proc. IMechE Part G, vol. 219, pp. 393-410, 2005.

[6] G. F. Syms, "Numerical simulation of frigate airwakes", *International Journal of Computational Fluid Dynamics*, vol. 18, no. 6, pp. 199-207, 2004.

[7] W. Yuan, R. Lee and A. Wall, "Simulation of unsteady ship airwakes using OpenFOAM", *30th Congress of the International Council of the Aeronautical Sciences*, Daejon, Korea, 2016.

[8] W. Yuan, A. Wall and R. Lee, "Combined numerical and experimental simulations of unsteady ship airwakes", *Computers & Fluids*, vol. 172, pp. 29-53, 2018.

[9] W. Yuan, A. Wall and R. Lee, "Simulations of unsteady airwakes behind ships in motion", *31st Congress International Council of the Aeronautical Sciences*, Belo Horizonte, Brazil, 2018.

[10] B. T. Cheney and S. J. Zan, "CFD code validation data and flow topology for the technical co-operation program AER-TP2 Simple Frigate Shape", *National Research Council*, Canada, Report LTR-A-035, 1999.

[11] K. R. Reddy, R. Toffoletto and K. R. W. Jones, "Numerical simulation of ship airwake", *Computers & Fluids*, vol. 29, pp. 451-465, 2000.

[12] N. H. Wakefield, S. J. Newman and P. A. Wilson, "Helicopter flight around a ship's superstructure", *Journal of Aerospace Engineering*, Proc Instn Mech Engrs, vol. 216, part G, no. 01801, pp. 13-28, 2002.

[13] R. Bardera-Mora, "Experimental investigation of the flow on a Simple Frigate Shape (SFS)", *The Scientific World Journal*, vol. 2014, no. 818132, 2014.

[14] D. Lindon and B. Thornber, "Quantifying uncertainty in turbulence resolving ship airwake simulations", *Ocean Engineering*, vol. 229, no. 108983, 2021.

[15] A. Zamiri and J. T. Chung, "Numerical evaluation of wind direction effects on the turbulence aerodynamics of a ship airwake", *Ocean Engineering*, vol. 284, no. 115104, 2023.

[16] G. F. Syms, "Simulation of simplified-frigate airwakes using a Lattice-Boltzmann method", *Journal of Wind Engineering and Industrial Aerodynamics*, vol. 96, no. 6, pp. 1197-1206, 2008.

[17] F. Zhang, H. Xu and N. Ball, "Numerical simulation of unsteady flow over SFS2 ship model", *AIAA Aerospace Sciences Meeting*, Orlando, Florida, vol. 47, AIAA 2009-81, no. 090081, 2009.

[18] J. S. Forrest and I. Owen, "An investigation of ship airwakes using Detached-Eddy Simulation", *Computers & Fluids*, Vol. 39, pp. 656-673, 2009.

[19] J. S. Forrest, C. H. Kääriä and I. Owen, "Determining the impact of hangar-edge modifications on ship-helicopter operations using offline and piloted helicopter flight simulation", *American Helicopter Society*, 66th Annual Forum & Technology Display, 2010.

[20] J. S. Forrest, C. H. Kääriä and I. Owen, "Evaluating ship superstructure aerodynamics for maritime helicopter operations through CFD and flight simulation", *Aeronautical Journal*, vol. 120, no. 1236, pp. 1578-1603, 2016.

[21] C. H. Kääriä, Y. Wang, M. D. White and I. Owen, "An experimental technique for evaluating the aerodynamic impact of ship superstructures on helicopter operations", *Ocean Engineering*, vol. 61, pp. 97-108, 2013.

[22] S. Shukla, S. S. Sinha and S. N. Singh, "Ship-helo coupled airwake aerodynamics: a comprehensive review", *Prog Aero Sci*, vol.106, pp. 71-107, 2019.

[23] S. Shukla, S. S. Sinha and S. N. Singh, "An investigation of ship airwakes by scale adaptive simulation" the *International Journal on Marine Navigation and Safety of Sea Transportation*, vol.1 4, no. 2, pp. 471-476, 2020.

[24] S. Shukla, S. S. Sinha, S. N. Singh and R. Vijayakumar, "A conceptual method to assess ship-helicopter dynamic interface", *Journal of Aerospace Engineering*, Proc IMechE Part G, vol. 234, no. 5, pp. 1092-1116, 2020.

[25] S. Shukla, S. S. Sinha, S. N. Singh and R. Vijayakumar, "Comparative assessment of URANS, SAS and DES turbulence modeling in the predictions of massively separated ship airwake characteristics", *Ocean Engineering*, vol. 229, no. 108954, 2021.

[26] F. R. Menter and Y. Egorov, "Scale-Adaptive Simulation method for unsteady flow predictions. Part 1: theory and model description", *Journal Flow Turbulence and Combustion*. vol. 85, pp. 113-138, 2010.

[27] Y. Egorov, F. R. Menter and D. Cokljat, "Scale-Adaptive Simulation method for unsteady flow predictions. Part 2: Application to Aerodynamic Flows", *Flow, Turbulence and Combustion*, vol. 85, pp. 139-165, 2010.

[28] P. R. Spalart, W. Jou, M. Strelets and S. Allmaras, "Comments on the feasibility of LES for wings and on a hybrid RANS/LES approach", *1st AFOSR Int. Conf. on DNS/LES*, 1997.

[29] P. R. Spalart, "Strategies for turbulence modelling and simulations", *Int. J. Heat Fluid Flow*, vol. 21, p. 2, 2000.

[30] F. R. Menter and M. Kuntz, "Adaptation of eddy-viscosity turbulence models to unsteady separated flow behind vehicles", *Proc. Conf. The Aerodynamics of Heavy Vehicles: Trucks, Busses and Trains*, Springer, Berlin, Heidelberg, pp. 339-352, 2003.

[31] P. R. Spalart, S. Deck, M. Shur, K. Squires, M. Strelets and A. Travin, "A new version of Detached Eddy Simulation resistant to ambiguous grid densities", *Journal of Theorotical Computational Fluid Dynamics*, vol. 20, pp. 181-195, 2006.

[32] F. R. Menter, "Stress-Blended Eddy Simulation (SBES) - a new paradigm in hybrid RANS-LES modeling", *Notes on Numerical Fluid*

Mechanics and Multidisciplinary Design, Springer International Publishing AG. Ansys Germany GmbH, no. 137, 2018.

[33] F. R. Menter, "Best practice: Scale-Resolving Simulations in ANSYS CFD", *Ansys Germany GmbH*, Version 1.0, 2012.

[34] R. G. Lee, "SFS 2 Code Validation Data Update", *TTCP AER TP 2 Dynamic Interface Workshop, 2003*, Patuxent River, USA, 2007.

[35] J. Jeong and F. Hussain, "On the identification of a vortex", *Journal of Fluid Mechanics*, vol. 285, pp. 69-94, 1995.